Macromolecules

pubs.acs.org/Macromolecules Article

Design, Synthesis, and Characterization of Semiconducting Polymers Incorporating a Ring-like Ureidopyrimidinone (UPy) Quadruple Hydrogen Bonding Structure

Xiaohong Wang, Chenyin Xu, Ning Xu, Longlong Jiang, Yunfei Wang, Fan Ni, Guobing Zhang, Xiaodan Gu, and Longzhen Qiu*

Cite This: *Macromolecules* 2023, 56, 5369−5380 Read Online

ACCESS | Metrics & More | Article Recommendations | Supporting Information

ABSTRACT: Introducing hydrogen bonding structures into semiconducting polymers is an effective method to enhance the intra/interchain interactions and improve the overall performance of the polymer. In this study, diketopyrrolopyrrole (DPP)-based random copolymers with quadruple hydrogen bonding in the backbone are constructed by the copolymerization of a rationally designed ring-like tetrahydrogen-bonded ureidopyrimidinone (UPy) with alkyl chain-substituted DPP using a new design strategy via intramolecular hydrogen bonding. Specifically, ring-like UPy structures with different ratios were introduced into DPP-based conjugated polymers by the Stille coupling. The electrical and mechanical properties of the resulting series polymers were characterized before and after stretching. The copolymer's tensile properties were improved owing to the introduction of the ring-like UPy unit, with 27.9% mobility retention under 100% stretching. More importantly, intramolecular quadruple hydrogen bonding was unprecedentedly introduced into the backbone of conjugated polymers, developing a new strategy for the introduction of multiple intramolecular hydrogen bonds into conjugated polymers conveniently and, more promisingly, enriching structural types of stretchable semiconductor polymers.

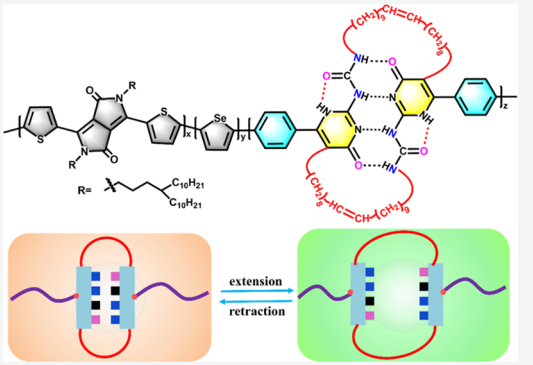

INTRODUCTION

As a new generation of semiconductor materials, conjugated polymers have attracted immense attention in the past decades because of their promise for applications in organic field-effect transistors (OFETs), organic solar cells (OSCs), and organic light-emitting diodes (OLEDs).[1−10] Introduction of hydrogen bonding interactions in conjugated polymer systems is a successful strategy for molecular design.[11,12] Hydrogen bonding can precisely regulate the polymer conformation because of its controlled strength and orientation.[13] In addition, hydrogen bonding is widely utilized to improve the planarity and rigidity of polymers through intra- and intermolecular noncovalent interactions, thereby improving interchain $\pi-\pi$ stacking and charge-transport properties.[14−16]

Typically, hydrogen bonds are introduced into both the polymer backbone[17−21] and side chains.[22−28] In the side chain, hydrogen bonds are usually introduced to enhance the interaction between chains and improve the electrical and mechanical properties. Several design strategies for introducing hydrogen bonding into the side chain have also been reported, including the introduction of amide, urea, and thymine group. By copolymerizing urea-based side chains with alkyl chains in different proportions, Zhang et al. reported that the hole mobility of the polymer films could be as high as 13.1 $cm^2 V^{-1} s^{-1}$ with the introduction of 10 mol % of urea-based side chains. The interaction between chains led to better mechanical properties and self-healing function in the materials.[22] Oh et al. synthesized DPP-based conjugated polymers containing polyurethane side chains that demonstrated excellent stretchability under an external strain of 100%, without any deterioration of electrical properties of organic transistors. The material also exhibited self-healing properties, capable of repairing cracks and restoring their electrical properties after treatment.[25]

Several design strategies for introducing hydrogen bonding into the backbone have also been reported, including incorporation of heteroatoms,[29,30] modulation of flanking structures,[31−33] selection of suitable donor units,[34−36] and introduction of structures that can form intermolecular hydrogen bonds.[17,37] For example, Yu et al. developed two donor−acceptor copolymers based on fluorinated dithiophene ethylene building blocks with prominent intramolecular C−

Received: March 9, 2023
Revised: June 2, 2023
Published: July 11, 2023

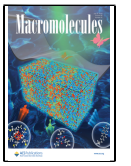

https://doi.org/10.1021/acs.macromol.3c00443
Macromolecules 2023, 56, 5369−5380

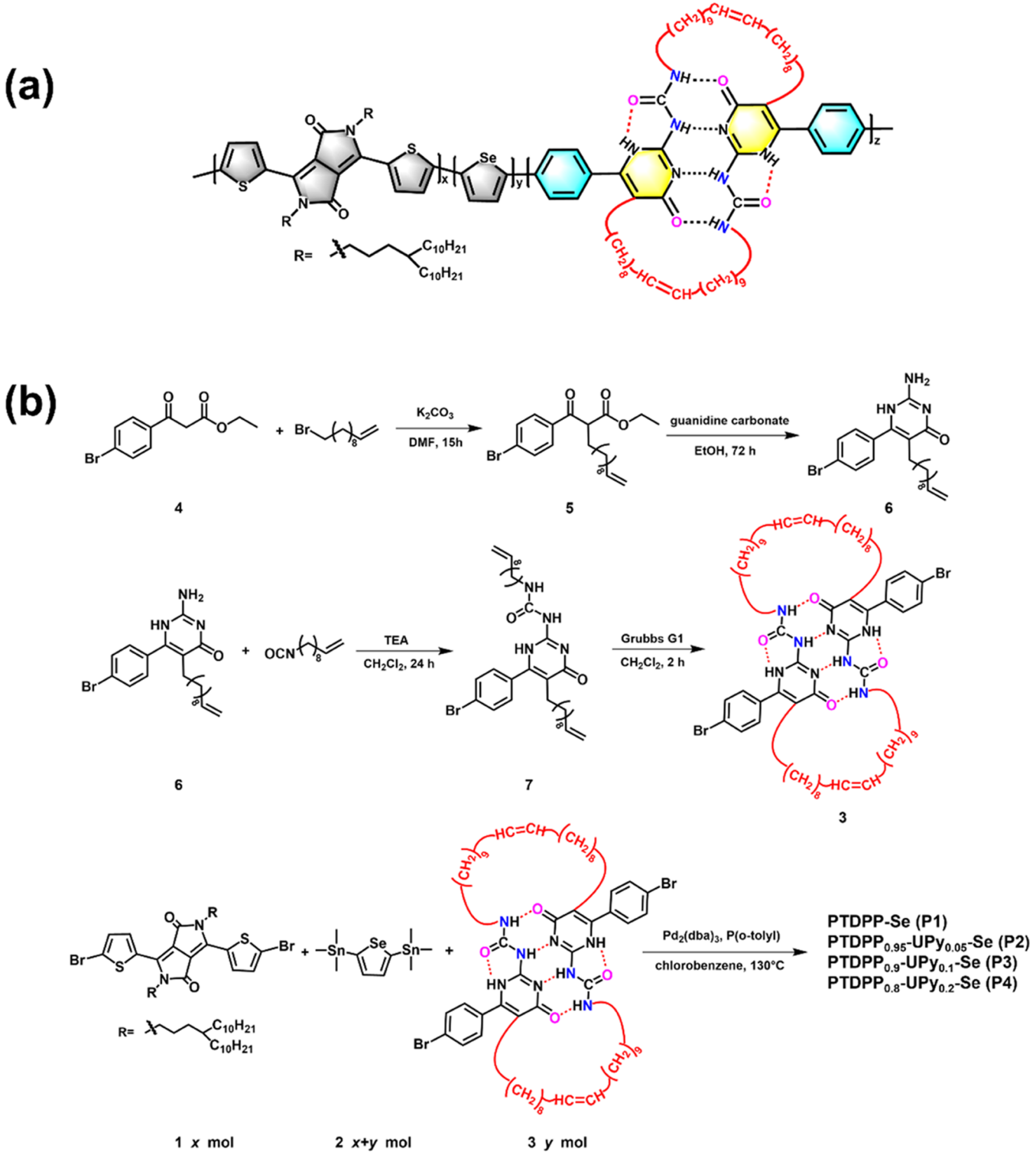

Figure 1. (a) Schematic of the polymers based on the UPy structure. (b) Synthetic approaches for monomers and polymers based on the UPy structure.

H···O and C−H···F interactions, leading to a more rigid and planar molecular backbone, achieving a high electron mobility of 3.2 cm^2 V^{-1} s^{-1}.[38] Bao et al. reported that inserting 2,6-pyridine dicarboxamide (PDCA) into the polymer backbone can reduce the overall backbone stiffness and crystallinity of the polymer film and provide an additional energy dissipation mechanism via the breaking of the dynamic noncovalent bonds (hydrogen bonds) in PDCA, thus improving the stretchability of the materials.[17] Despite significant progress in the design of polymeric semiconductor materials as well as device structures based on hydrogen bonding, most of the hydrogen bonding applied so far are mainly mono-(amide) and di-(urea) bonds, generating limited intermolecular forces. In contrast, stronger intermolecular forces are present in quadruple hydrogen bonding,[39−41] leading to the significant increase in ductility and tensile strength, hence opening a wide range of

https://doi.org/10.1021/acs.macromol.3c00443
Macromolecules 2023, 56, 5369−5380

applications as cross-linkers,[42,43] self-healing elastomers,[44−46] and self-healing thin-film electrodes.[47] However, the introduction of ring-like quadruple hydrogen bonding into the backbone of conjugated polymers has not been reported.

Inspired by the previous design method, a new method to introduce a ring-like ureidopyrimidinone (UPy) quadruple hydrogen bonding structure composed of multiple alkyl groups into the conjugated polymer was presented; this is also the first report of the introduction of intramolecular quadruple hydrogen bonding into a conjugated polymer. The UPy unit content was controlled from 5 to 20 mol % for random copolymerization with DPP-based conjugated polymers. In addition, the effect of the UPy unit on the electrical and mechanical properties of the conjugated polymers was investigated. The UPy unit with the ring-like quadruple hydrogen bonding structure dissipated the stress by breaking the hydrogen bonds under the stretching of the films, and this method provides a new route for developing highly stretchable conjugated polymers.

RESULTS AND DISCUSSION

Synthesis of Monomers and Polymers. Figure 1a shows the structure of the copolymers. Figure 1b outlines the synthetic routes for the conjugated polymers named as PTDPP-Se (P1), $PTDPP_{0.95}$-$UPy_{0.05}$-Se (P2), $PTDPP_{0.9}$-$UPy_{0.1}$-Se (P3), and $PTDPP_{0.8}$-$UPy_{0.2}$-Se (P4), with different ratios of "ring-like" quadruple hydrogen bonding structures introduced into the backbone. Compounds **1**, **2**, and **4** are commercially available and can be used directly without further purification. Monomer **3** was synthesized in a stepwise manner starting from monomer **4**. Monomer **4** underwent nucleophilic substitution with bromoundecene, affording monomer 5 in 48% yield, followed by the addition of guanidine carbonate under ethanol reflux to produce monomer **6**; monomer **6** underwent an addition reaction with undecylenyl isocyanate to afford monomer **7** containing urea groups. The final cyclic monomer **3** was synthesized by olefin complexation under the action of the Grubbs generation catalyst. The series conjugated polymers were synthesized by copolymerization via the Stille coupling using compounds **1**, **2**, and **3**.

Conjugated polymers P2, P3, and P4 were obtained by variation in the molar equivalence ratio of the mediated product **3** from 0.05 to 0.1 and 0.2 mol %. For comparison, polymer P1 which lacks the UPy structure was also prepared. Briefly, after the completion of polymerization, methanol was added to the reaction solution to precipitate the product. The precipitated product was then subjected to Soxhlet extraction with methanol, acetone, and hexane to remove unreacted monomers and oligomers. The P1−P4 polymers were finally obtained by extraction with chloroform and then again precipitated in methanol with yields of 80, 70, 70, and 75%, respectively. The chemical structures of the monomers and polymers were determined by ^{1}H NMR spectroscopy and mass spectrometry (see the Experimental Section and Supporting Information Figures S11−S15). To demonstrate the presence of quadruple hydrogen bonding, we conducted a comparative analysis of the Fourier transform infrared (FT-IR) spectra for the UPy, P1, and P4 samples. As depicted in Figure S1a, compared to P1, P4 shows new vibration peaks at 1257, 1580, 1690, 3149, and 3211 cm^{-1}, all of which occur in the IR spectrum of the ring-like UPy monomer. The stretching vibrational peaks at 1690 cm^{-1} corresponding to hydrogen bonding in C═O and at 3211 and 3149 cm^{-1} corresponding to hydrogen bonding in N−H demonstrate the existence of quadruple hydrogen bonding in the polymer backbone. Furthermore, the ^{1}H NMR spectra of the UPy and P4 samples were compared, as illustrated in Figure S1b. Notably, peaks with chemical shifts of 13.03 and 11.98 ppm were observed in the ^{1}H NMR spectrum of the P4 sample, corresponding to the N−H chemical shifts associated with hydrogen bonding interactions. Additionally, a peak at 10.16 ppm was identified, representing the N−H chemical shift attributed to the carbonyl group. These findings further support the presence of UPy quadruple hydrogen bonding interactions within the molecular structure of P4. Table 1 shows the basic physicochemical properties of the four polymers. The number-average molecular weights of P1−P4 polymers were 75.2, 57.4, 43.0, and 53.9 kDa, with polydispersity (PDI) values of 2.76, 2.72, 2.87, and 2.63, respectively, as measured by gel permeation chromatography in chloroform (Figure S2).

Table 1. Basic Physicochemical Properties of Polymers P1−P4

				λ_{max} (nm)[c]			
polymer	M_n[a] (kDa)	PDI[b]	T_d (°C)	solution	film	E_g^{cv} (eV)[d]	E_g^{opt} (eV)[e]
P1	75.2	2.76	393	848	869	1.94	1.31
P2	57.4	2.72	389	847	857	1.95	1.30
P3	43.0	2.87	373	839	848	1.93	1.31
P4	53.9	2.63	337	812	855	1.87	1.32

[a]Number-average molecular weight and weight-average molecular weight estimated by gel permeation chromatography in chloroform using polystyrene as the standard. [b]Weight dispersity defined as M_w/M_n. [c]Maxima absorption of UV−vis in $CHCl_3$ solutions (1.0×10^{-5} M for each polymer) and the spin-coated thin films. [d]Based on cyclic voltammetry. [e]Based on the UV−vis absorption spectral data.

Electrochemical and Optical Properties. The cyclic voltammetry curves of P2, P3, and P4 films were obtained by electrochemical workstation tests, and the onset oxidation and reduction potentials were used to estimate the highest occupied molecular orbital (HOMO) and lowest unoccupied molecular orbital (LUMO) energy levels, as shown in Table 1, Figures 2c, and S3. The HOMO and LUMO energy levels were calculated on the basis of eqs 1 and 2

$$E_{HOMO} = -(E_{ox}\text{onset} + 4.75\ \text{eV}) \quad (1)$$

$$E_{LUMO} = -(E_{red}\text{onset} + 4.75\ \text{eV}) \quad (2)$$

For comparison, the HOMO and LUMO energy levels of P1 also were measured in the same manner and are shown in Table 1 and Figure 2c. As demonstrated in Figure 2c, the HOMO and LUMO energy levels of P1−P4 were −5.22, −5.24, −5.23, −5.18, and −3.28, −3.29, −3.30, −3.31 eV, respectively. It can be found that the energy levels of the four polymers are similar due to the similarity of the backbone structures of the four polymers.

To investigate the effect of the UPy content on the aggregation state of polymers, UV−vis absorption spectra of the four polymers were recorded in the solution and film states (Figure 2a,b). All of the polymers (P1−P4) exhibited two absorption bands: a higher-energy absorption band at 400−450 nm, corresponding to $\pi-\pi^*$ transitions, and a band at 600−850 nm with two vibrational peaks (0−0 and 0−1) attributed to donor−acceptor charge transfer. As the UPy unit

https://doi.org/10.1021/acs.macromol.3c00443
Macromolecules 2023, 56, 5369−5380

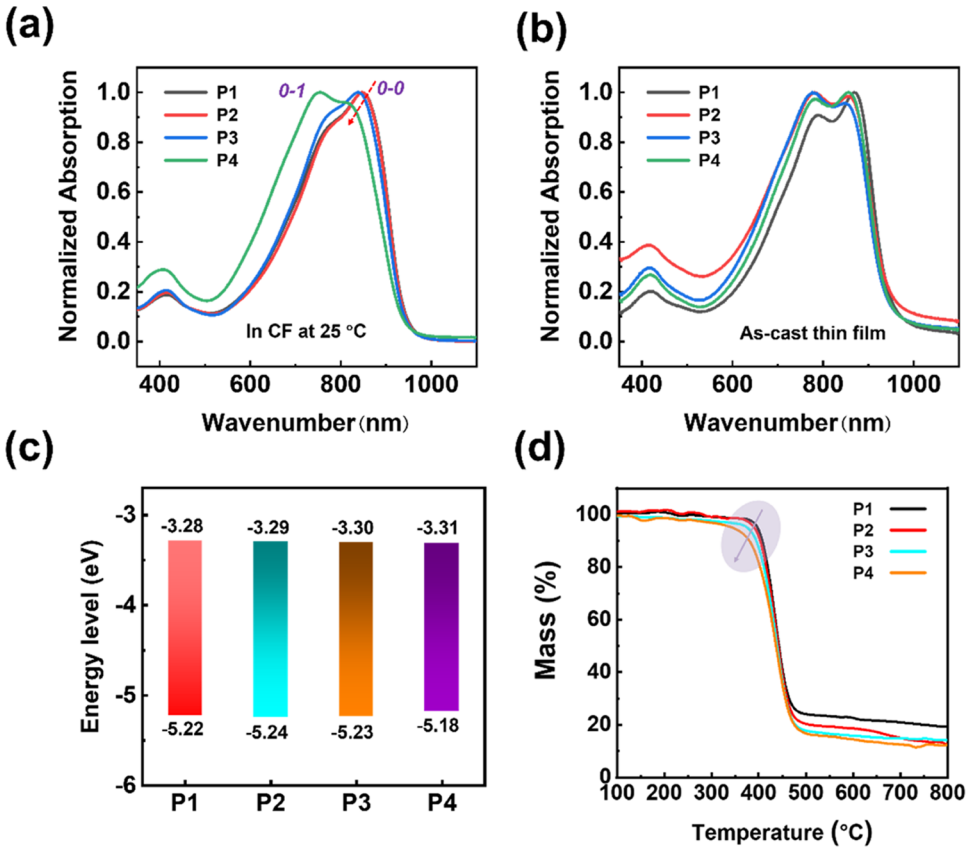

Figure 2. Normalized ultraviolet−visible (UV−vis) absorption spectra of polymers P1−P4. (a) Chloroform solution at room temperature. (b) Thin films spin-coated from chloroform (5 mg mL^{-1}). (c) HOMO/LUMO energy levels obtained by the electrochemical testing of polymers P1−P4. (d) Thermogravimetric analysis curves of polymers P1−P4.

in the polymer increased, the ring-like structure which prevents the aggregation of molecules, the intensity of the 0−0 peak in polymer solutions gradually decreased from P1 to P4. In addition, the maximum absorption peak of the polymer in chloroform solution continuously blue-shifted from 847 nm for P1 to 808 nm for P4 due to the disruption of the backbone conjugated structure. For thin films, the value of 0−0 transition peak has a tendency to decrease and then increase slightly. This may be due to the introduction of the UPy unit leading to the formation of the phase separation structure. According to the thermogravimetric analysis data shown in Figure 2d, the thermal decomposition temperatures (measured at 5% weight loss) of P1, P2, P3, and P4 were greater than 330 °C, which ensured sufficiently thermal stability for applications such as organic thin-film transistors and other electronic devices.

Organic Field-Effect Transistor Characteristics of the Polymers. To investigate the effect of the introduction of ring-like quadruple hydrogen bonding in the backbone on the charge-transport properties of PTDPP-Se spin-coated films, bottom-gate top-contact (BGTC) OFETs were prepared by conventional device fabrication steps, and detailed steps are described in the Experimental Section. The electrical properties of these conjugated polymer films were tested under ambient conditions. Figure 3a−h shows the transfer and output characteristic curves of the OFETs of these conjugated polymer films at room temperature and after thermal annealing at 90, 150, and 210 °C, respectively (where the output characteristic curves were selected at their optimal annealing temperatures). Figure 3i−k shows the variation of hole mobility (μ_h), on/off current ratio (I_{on}/I_{off}), and threshold voltage (V_{Th}) at different annealing temperatures. All of the polymers exhibited distinct p-type transport characteristics. Table S1 summarizes the μ_h, V_{Th}, and I_{on}/I_{off} data extracted by the linear fitting of the transfer curves.

As the UPy content increased, the mobilities of the polymer films decreased from 0.55 $cm^2\ V^{-1}\ s^{-1}$ of P1 to 0.13 $cm^2\ V^{-1}\ s^{-1}$ of P4 because of the nonconjugated structure of the ring-like quadruple hydrogen bonding, which led to the breaking of the backbone conjugation. This trend was observed for polymer films annealed at different temperatures. Specifically, the P1 polymer without the UPy structure exhibited the maximum mobility value of 0.85 $cm^2\ V^{-1}\ s^{-1}$ after annealing at 90 °C, while P2, P3, and P4 with the UPy structure exhibited the best electrical properties after annealing at 150 °C. This result is likely related to the formation of higher barriers to molecular chain motion with the introduction of the strong interacting quadruple hydrogen bonging structures. Hence, higher temperatures are required to induce the movement of molecular chains. The annealing temperature crucially affects the mobility of the conjugated polymers. The mobility of all films initially increased and then decreased with increasing annealing temperature. This effect was mainly related to the promotion of molecular chain rearrangement by the increase in the temperature, thereby facilitating closer intermolecular stacking and charge transfer. However, as the annealing temperature reached 210 °C, the thin film showed apparent holes, which hindering charge transfer, resulting in decreased mobility. Therefore, selecting a suitable annealing temperature

https://doi.org/10.1021/acs.macromol.3c00443
Macromolecules 2023, 56, 5369−5380

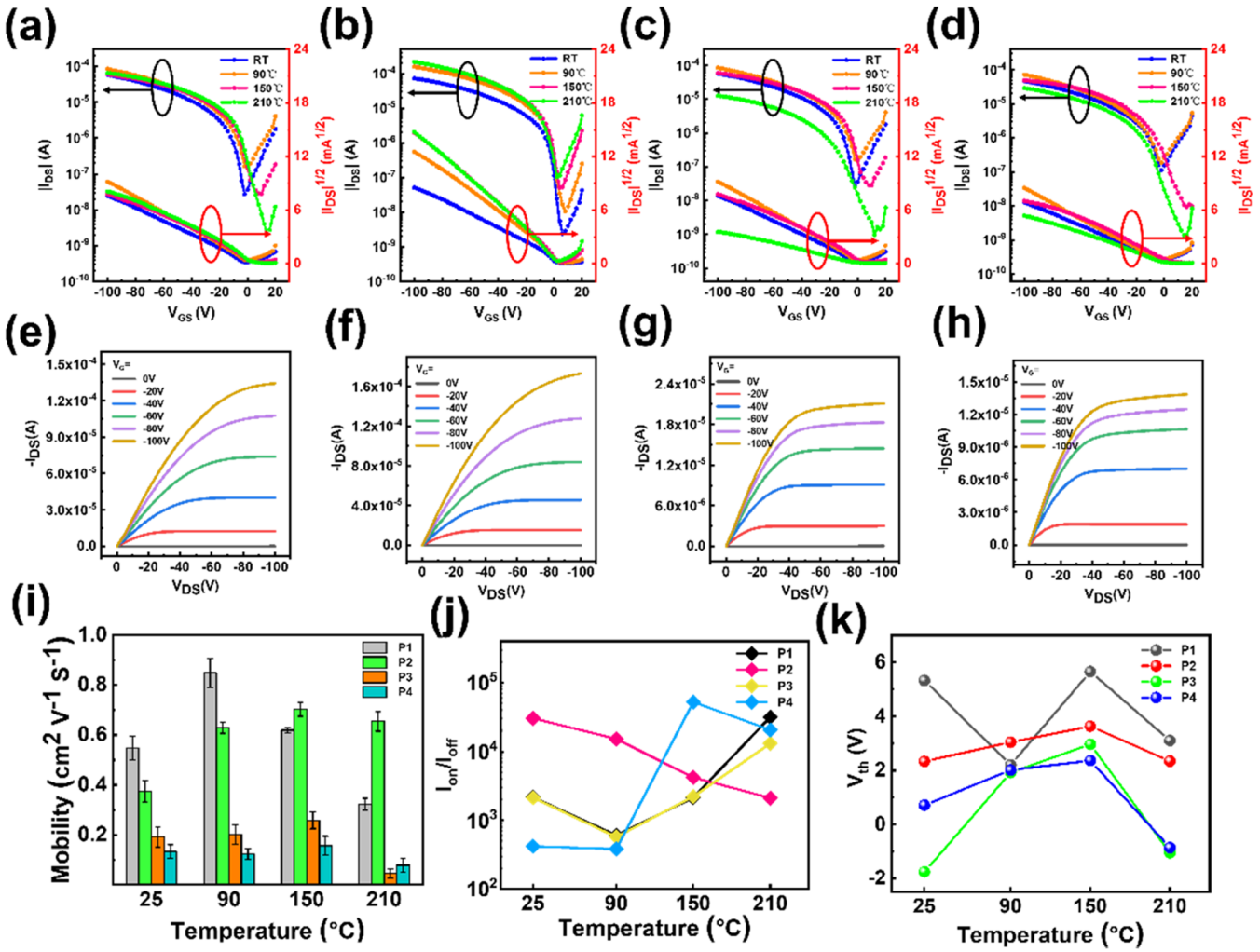

Figure 3. Electrical properties of polymers P1−P4 at different annealing temperatures. (a−d) Transfer curves of the OFET devices based on polymers P1−P4. (e−h) Output curves of the OFET devices based on polymers P1−P4 at the optimum annealing temperature. (i−k) Change curves of mobility, threshold voltage, and on/off current ratio as a function of the annealing temperature.

is crucial for the preparation of high-performance and highly stable FETs.

Morphologies and Microstructures of the P1−P4 Polymer Films. The effect of the introduction of quadruple hydrogen bonding on the crystalline structure and stacking pattern of the polymers before and after annealing was investigated using grazing incidence wide-angle X-ray scattering (GIWAXS). All four polymers exhibited significant (h00) diffraction peaks (Figure 4a), attributed to their lamellar packing structure. After annealing, the lamellar packing distance of four polymers became smaller, which is consistent with the improved electrical properties observed after annealing. The (010) diffraction peaks were observed in both in-plane and out-of-plane directions for the P1, P2, P3, and P4 polymer films before and after annealing, indicating the face-on and edge-on coexisting orientation of the molecules (Figure S5).[48,49] However, the in-plane (010) diffraction peaks of the annealed P2, P3, and P4 polymers were significantly sharper than that of P1, suggesting that the introduction of the quadruple hydrogen bonding structure renders a large coherence length of the polymer crystallites. Figure 4b,c shows the calculated $\pi-\pi$ stacking distances and full width at half-maximum (FWHM) values of the four polymers. After annealing, the $\pi-\pi$ stacking distance gradually increased, and the FWHM gradually decreased after the introduction of the quadruple hydrogen bonding structure. Specifically, the $\pi-\pi$ stacking distance increased from 3.62 Å for P1 to 3.64 Å for P4, and the FWHM decreased from 0.09 $Å^{-1}$ for P1 to 0.031 $Å^{-1}$ for P4 (see Supporting Information Table S2). This phenomenon indicated that the intermolecular interaction of quadruple hydrogen bonding is beneficial to the crystallinity of the polymers. There is a tendency for the $\pi-\pi$ stacking distance to decrease in annealed films compared to the films at room temperature, indicating that the molecular chains are more tightly packed, which is beneficial for charge transport.

To further investigate the effect of annealing on the electrical properties of several polymers, the structural information of films was obtained by atomic force microscopy (AFM). Figure 4d shows the AFM images of the P1 and P4 films at room temperature as well as at their respective optimal annealing temperatures. Compared to the P1 film, the P4 film comprised nanofiber structures at room temperature, which was possibly related to the introduction of quadruple hydrogen bonding in the P4 backbone. The intermolecular interactions resulting from the quadruple hydrogen bonding promoted the formation of a small amount of nanofibers that were interconnected within the film.[22] In addition, the P1 revealed no significant change in morphology and roughness when the film was

https://doi.org/10.1021/acs.macromol.3c00443
Macromolecules 2023, 56, 5369−5380

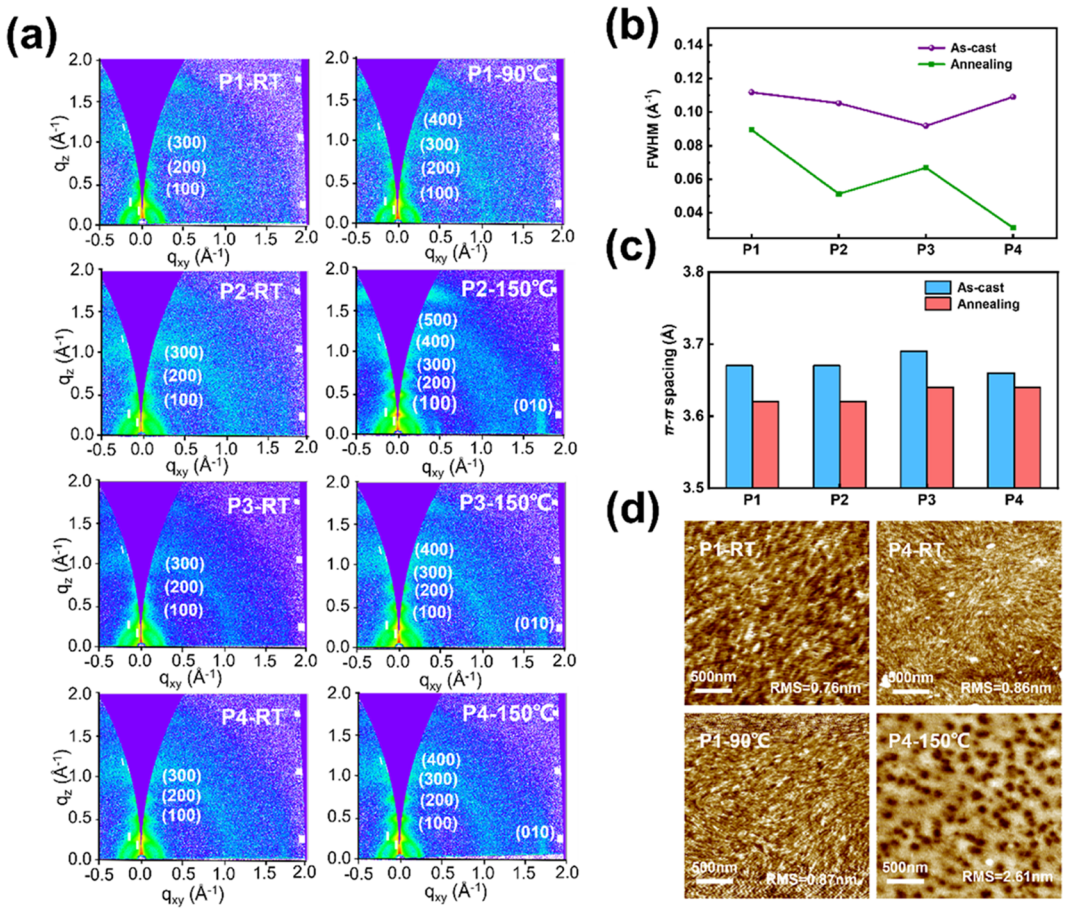

Figure 4. (a) GIWAX-2D patterns of the polymer films before and after annealing. (b, c) FWHM and $\pi-\pi$ stacking distance of the polymer films (30 nm in thickness) before and after annealing. (d) Atomic force microscopy (AFM) morphology of P1 and P4 films at different temperatures.

annealed at 90 °C, while the fiber structure in the P4 almost disappeared after annealing at 150 °C, and a clear pore structure was observed. The appearance of the pore structure may be related to the rearrangement of the molecular chains at high temperatures. This phenomenon became more obvious for polymer films annealed at 210 °C. This morphological change would be detrimental to charge transport (Figures 4d and S6).

Mechanical Properties of Polymer Films. Figure 5a shows the transfer and stretching process of the prepared films. The optical microscopy (OM) images of P1, P2, P3, and P4 films after 30 and 100% stretching are shown in Figure 5b; P1 films exhibited large and dense cracks after stretching to 100%, while P4 films exhibited relatively fewer cracks. Figure 5c shows the AFM images of P1, P2, P3, and P4 films after 30 and 100% stretching. All polymers exhibited cracks after 30% stretching, indicating that the crack onset strain is less than 30%. In comparison to the wide cracks of the P1, P2, P3 films, P4 films exhibited fewer and smaller cracks, indicating that the intramolecular and intermolecular interaction forces introduced by quadruple hydrogen bonding in the backbone can dissipate stress during the stretching process. Figures S7 and S8 show the film morphology of the four polymers at a strain ratio from 0 to 100%. In addition, to observe the film morphology at high resolution, we have used high-resolution field emission scanning electron microscopy (SEM) to observe the crack changes in the film during stretching (as shown in Figure S9).These results indicate that the introduction of ring-like quadruple hydrogen bonding can enhance the tensile properties of the films.[40,50]

To quantify the mechanical properties of P1−P4 polymer films under tensile strain, the dichroic ratio (R) was calculated from UV−vis spectroscopy obtained under linearly polarized light (Figure 6a). The absorbance of linearly polarized light parallel to the strain direction increased relative to the absorbance of the perpendicular incident light to the strain direction over the entire spectral range for all P1−P4 films. R was associated with the alignment of the polymer backbones along the strain direction. The R values of P1−P4 films in the stretched to the 100% state were 1.16, 1.28, 1.26, and 1.42, respectively. The R value of the P4 film was found to be linearly dependent on the level of applied strain and increased from 1.0 to 1.4 with the increase in the strain ratio to 100%, indicative of the improved ductility of the thin film (Figure 6b). The higher R value for the P4 film compared with those for the P1, P2, and P3 films indicated better polymer chain alignment under the same strain ratio, suggestive of the high mechanical tolerance of the P4 films. This result was consistent with the OM and AFM results, indicating that the introduction of ring-like quadruple hydrogen bonding facilitates better chain alignment during stretching and renders better mechanical resistance.

The elastic moduli of the P1−P4 films were calculated by eq 3

https://doi.org/10.1021/acs.macromol.3c00443
Macromolecules 2023, 56, 5369−5380

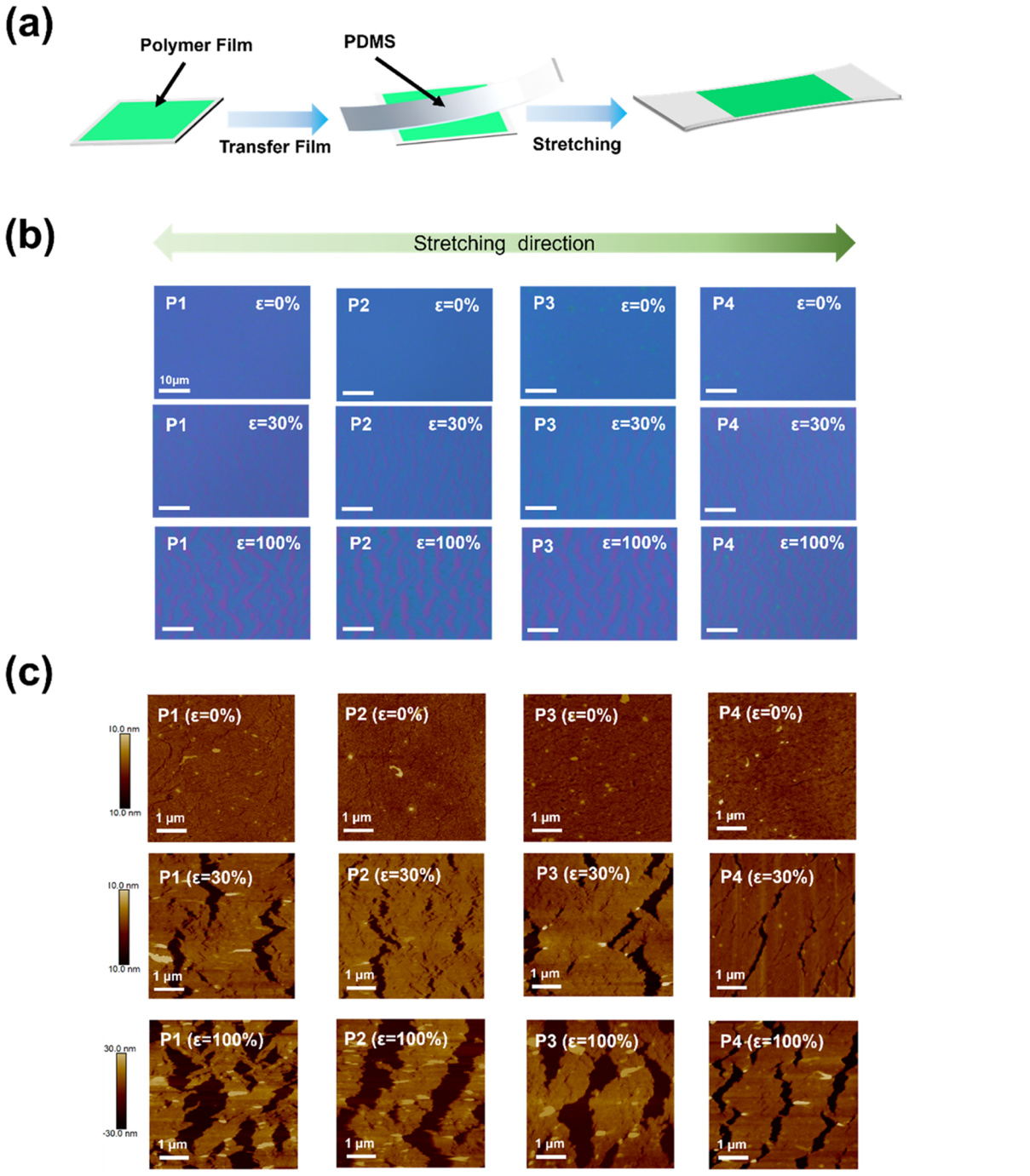

Figure 5. (a) Schematic of the preparation process for the stretched films. (b, c) Optical and AFM images of the P1−P4 films at different stretching ratios. The color scale of the AFM images represents relative height.

$$\frac{E_f}{1-\nu_f^2} = \frac{3E_s}{1-\nu_s^2}\left(\frac{\lambda}{2\pi d}\right)^3 \quad (3)$$

where V_f and V_s represent the Poisson's ratios of the polymer film and poly(dimethylsiloxane) (PDMS), respectively, λ and d represent the periodic bending wavelength and thickness of the film, respectively, E_s represents the modulus of elasticity of the polymer film, and E_f represents the calculated modulus of elasticity of the film.[51,52] The elastic moduli values of the P1−P4 films was 890 ± 45, 843 ± 62, 687 ± 53, and 404 ± 68 MPa, respectively (Figure 6c). Compared with that of P1, the elastic modulus of P4 decreased substantially due to the reduced crystallinity by the introduction of ring-like hydrogen bonding. Therefore, the introduction of ring-like quadruple hydrogen bonding leads to the decrease in the elastic modulus of the material and renders better tensile properties to the polymer films.

The electrical properties of the P1−P4 polymer films under different stretching ratios were further investigated using the OFET structures (Figure 7a). Changes in the charge-transport properties in the vertical and parallel directions to the stretching direction are shown in Figure 7b−e. As the stretching ratio increased, the mobility of the four polymers decreased significantly. The mobility of the P1 film decreased

https://doi.org/10.1021/acs.macromol.3c00443
Macromolecules 2023, 56, 5369−5380

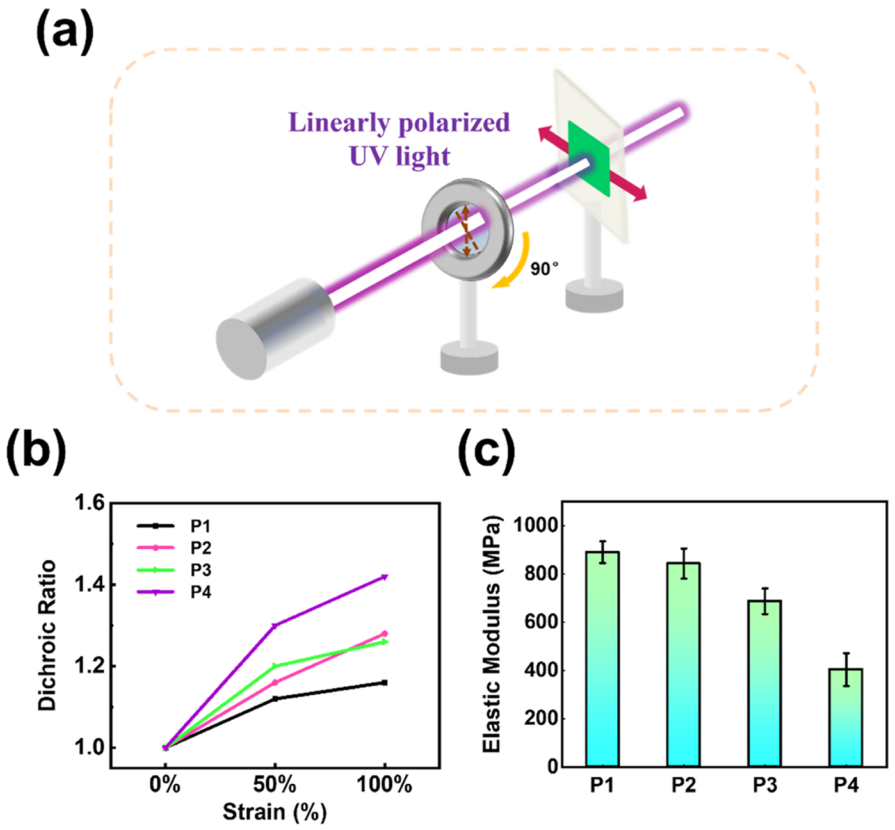

Figure 6. (a) Schematic of dichroic ratio (R) measurements from UV−vis spectroscopy obtained under linearly polarized light. (b) Dichroic ratios of polymers P1−P4 films at different strain ratios. (c) Calculated elastic moduli of P1−P4 polymer films (30 nm thickness) using the flexural method.

from 0.824 to 0.156 $cm^2\ V^{-1}\ s^{-1}$ in the vertical direction; in contrast, the electrical properties of P4 decreased slowly from 0.194 to 0.054 $cm^2\ V^{-1}\ s^{-1}$. Mobility retention for these four polymers after stretching was calculated to assess the ability of the polymers to maintain their electrical properties in the stretched state. The mobility retention values of the four polymers in the vertical direction were 18.9, 13.9, 17.4, and 27.9%, respectively. In the parallel direction, P4 still exhibited the highest mobility retention due to the prevention of further crack propagation during the stretching process owing to the presence of quadruple hydrogen bonding. This result revealed that the introduction of quadruple hydrogen bonding in the backbone can effectively dissipate stress,[53] reduce the number of cracks, and maintain the electrical properties. Based on the morphology of the four polymers after stretching, Figure 7f envisions the schematic of the dissipative stresses caused by the quadruple hydrogen bonding during stretching; the quadruple hydrogen bonding played a locking role to maintain the intrinsic conformation of the molecular chains during the stretching process. The quadruple hydrogen bond may open after stretching, and the ring may act as a protection to restore the quadruple hydrogen bonding. However, further studies need to be conducted to understand the mechanism of ring-like hydrogen bonding in the stretchable conjugated polymers and to improve the electrical characteristics of the stretchable conjugated polymers with hydrogen bonding, which in turn can facilitate the application of the stretchable conjugated polymers in flexible electronics.

CONCLUSIONS

In this study, four polymers, namely, P1, P2, P3, and P4, were successfully prepared using ring-like UPy quadruple hydrogen bonding units. The effect of quadruple hydrogen bonding content on the photoelectric and mechanical properties of DPP-based conjugated polymers was investigated. The introduction of the ring-like quadruple hydrogen bonding structure led to breaking the conjugation of the backbone; therefore, the electrical properties of P4 are lower than P1. However, P4 exhibited improved mechanical properties at a UPy content of 20% compared to P1. This improvement is probably related to the intermolecular interaction force caused by quadruple hydrogen bonding in the polymer and the stress dissipation by the long ring-like chains in the backbone of the polymer during the stretching process. In conclusion, the introduction of a ring-like quadruple hydrogen bonding structure in the backbone is a novel molecular design strategy for semiconductor polymers. The proposed quadruple hydrogen bonding design strategy and synthesis route in this study provide new ideas for the further development of functional semiconductor polymer materials.

EXPERIMENTAL SECTION

Materials and Characterization Methods. Most of the chemicals (not specified) are commercially available and can be used directly without further purification. Synthetic procedures and characterization techniques for monomers and polymers are available in the Supporting Information.

Preparation and Characterization of OFET Devices. Bottom-gate top-contact (BGTC) OFET devices were prepared, with n-doped Si and SiO_2 as the gate and dielectric layer, respectively, and the

https://doi.org/10.1021/acs.macromol.3c00443
Macromolecules 2023, 56, 5369−5380

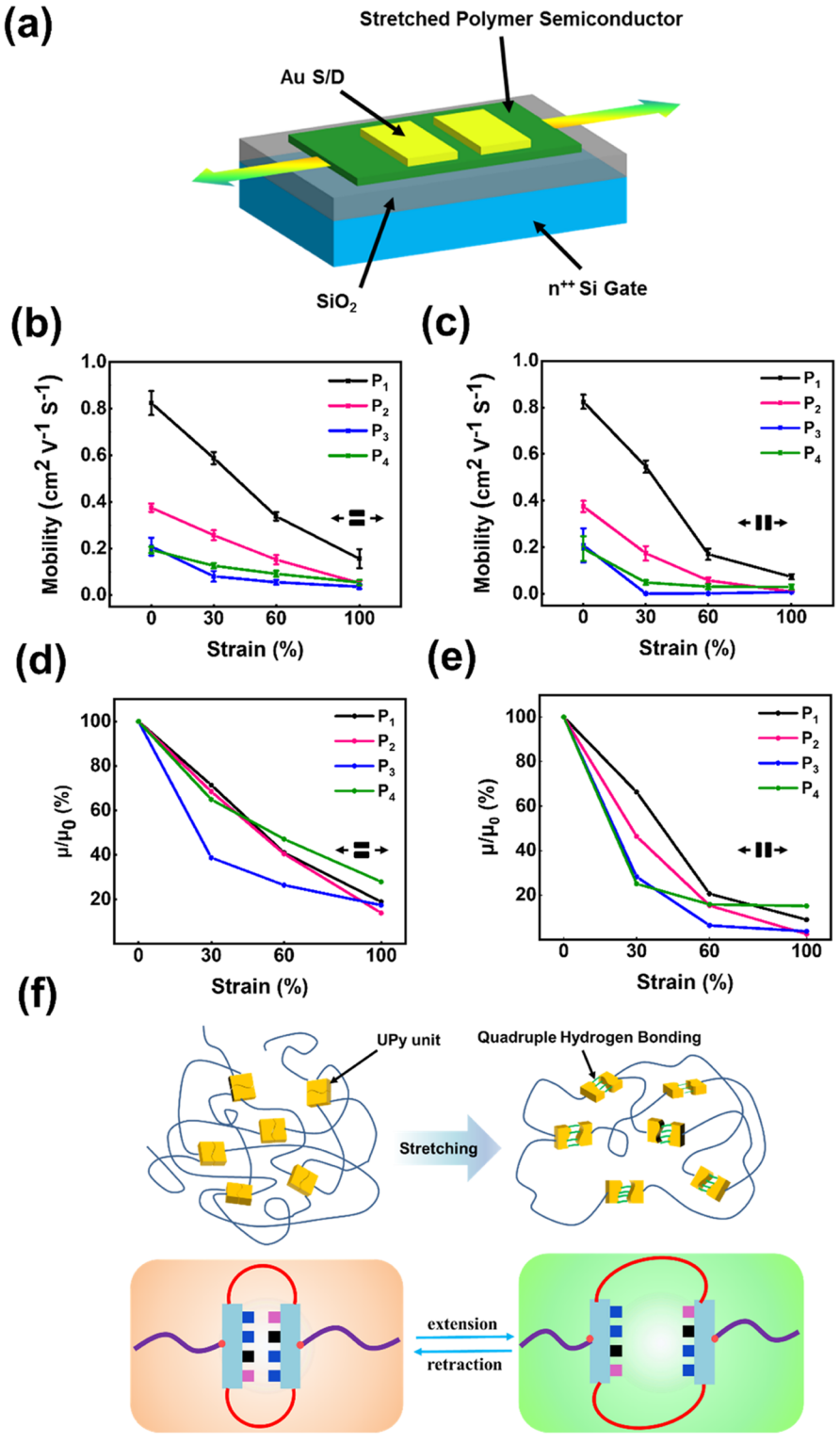

Figure 7. (a) Schematic of the bottom-gate top-contact transistor devices. (b, c) Mobility change in the vertical and parallel strain directions of the P1−P4 films. (d, e) Mobility retention under vertical and parallel strain directions of the P1−P4 films. (f) Mechanism of the dissipative stress process of the ring-like quadruple hydrogen bonding under extension and retraction.

formulated perfluoro(1-butenyl vinyl ether) polymer (CYTOP) solution was spin-coated on the SiO_2 surface. The polymers were dissolved in chloroform at a concentration of 5 mg mL^{-1} and spin-coated on CYTOP at 3000 rpm. Au was plated on the films by thermal evaporative deposition with a channel length and a width of 100 and 1000 μm, respectively. The mobility of the P1−P4 films were calculated by eq 4

$$I_{SD} = (W/2L)C_i\mu(V_G - V_{th})^2 \quad (4)$$

where I_{SD} is the source current, W and L are the width and length of the channel, respectively, C_i is the capacitance per unit area of the insulating layer, V_G is the gate voltage, and V_{th} is the threshold voltage.

Transfer and Stretching Process. The polymer films spin-coated on CYTOP were transferred down using PDMS, stretched at

https://doi.org/10.1021/acs.macromol.3c00443
Macromolecules 2023, 56, 5369−5380

different ratios (0, 30, 60, 100%), and then transferred to another SiO_2 substrate. The strained polymer films were coated with gold by a thermal evaporation deposition process with a channel length and width of 100 and 1000 μm, respectively.

■ ASSOCIATED CONTENT

Supporting Information

The Supporting Information is available free of charge at https://pubs.acs.org/doi/10.1021/acs.macromol.3c00443.

Characterization methods, GPC, synthesis of monomers and polymers, cyclic voltammogram, NMR images, OM, AFM, GIWAXS, and output curves (PDF)

■ AUTHOR INFORMATION

Corresponding Author

Longzhen Qiu − *National Engineering Lab of Special Display Technology, Special Display and Imaging Technology Innovation Center of Anhui Province, Academy of Opto-Electronic Technology, Hefei University of Technology, Hefei 230009, China; Anhui Province Key Laboratory of Measuring Theory and Precision Instrument, Intelligent Interconnected Systems Laboratory of Anhui Province, School of Instrument Science and Opto-Electronic Engineering, Hefei University of Technology, Hefei 230009, China;* orcid.org/0000-0002-8356-6303; Email: lzhqiu@hfut.edu.cn

Authors

Xiaohong Wang − *National Engineering Lab of Special Display Technology, Special Display and Imaging Technology Innovation Center of Anhui Province, Academy of Opto-Electronic Technology, Hefei University of Technology, Hefei 230009, China; Anhui Province Key Laboratory of Measuring Theory and Precision Instrument, Intelligent Interconnected Systems Laboratory of Anhui Province, School of Instrument Science and Opto-Electronic Engineering, Hefei University of Technology, Hefei 230009, China*

Chenyin Xu − *National Engineering Lab of Special Display Technology, Special Display and Imaging Technology Innovation Center of Anhui Province, Academy of Opto-Electronic Technology, Hefei University of Technology, Hefei 230009, China; Anhui Province Key Laboratory of Measuring Theory and Precision Instrument, Intelligent Interconnected Systems Laboratory of Anhui Province, School of Instrument Science and Opto-Electronic Engineering, Hefei University of Technology, Hefei 230009, China*

Ning Xu − *National Engineering Lab of Special Display Technology, Special Display and Imaging Technology Innovation Center of Anhui Province, Academy of Opto-Electronic Technology, Hefei University of Technology, Hefei 230009, China; Anhui Province Key Laboratory of Measuring Theory and Precision Instrument, Intelligent Interconnected Systems Laboratory of Anhui Province, School of Instrument Science and Opto-Electronic Engineering, Hefei University of Technology, Hefei 230009, China*

Longlong Jiang − *National Engineering Lab of Special Display Technology, Special Display and Imaging Technology Innovation Center of Anhui Province, Academy of Opto-Electronic Technology, Hefei University of Technology, Hefei 230009, China; Anhui Province Key Laboratory of Measuring Theory and Precision Instrument, Intelligent Interconnected Systems Laboratory of Anhui Province, School of Instrument Science and Opto-Electronic Engineering, Hefei University of Technology, Hefei 230009, China*

Yunfei Wang − *School of Polymer Science and Engineering, The University of Southern Mississippi, Hattiesburg, Mississippi 39406, United States;* orcid.org/0000-0001-7555-5308

Fan Ni − *National Engineering Lab of Special Display Technology, Special Display and Imaging Technology Innovation Center of Anhui Province, Academy of Opto-Electronic Technology, Hefei University of Technology, Hefei 230009, China; Anhui Province Key Laboratory of Measuring Theory and Precision Instrument, Intelligent Interconnected Systems Laboratory of Anhui Province, School of Instrument Science and Opto-Electronic Engineering, Hefei University of Technology, Hefei 230009, China*

Guobing Zhang − *National Engineering Lab of Special Display Technology, Special Display and Imaging Technology Innovation Center of Anhui Province, Academy of Opto-Electronic Technology, Hefei University of Technology, Hefei 230009, China; Anhui Province Key Laboratory of Measuring Theory and Precision Instrument, Intelligent Interconnected Systems Laboratory of Anhui Province, School of Instrument Science and Opto-Electronic Engineering, Hefei University of Technology, Hefei 230009, China;* orcid.org/0000-0001-6053-2015

Xiaodan Gu − *School of Polymer Science and Engineering, The University of Southern Mississippi, Hattiesburg, Mississippi 39406, United States;* orcid.org/0000-0002-1123-3673

Complete contact information is available at: https://pubs.acs.org/10.1021/acs.macromol.3c00443

Notes

The authors declare no competing financial interest.

■ ACKNOWLEDGMENTS

This study was supported by the National Natural Science Foundation of China (NSFC, Grant Nos. 52273172, 62274053), the National Key Research and Development Program of China (2022YFE0198200), the Major Science and Technology Project of Anhui Province (2021e03020007), and the Natural Science Foundation of Hefei (2022031, 2022002). X.G. and Y.W. thank the National Science Foundation for providing funding resource for the GIWAXS measurement under Award Number DMR-2047689.

■ REFERENCES

(1) Fratini, S.; Nikolka, M.; Salleo, A.; Schweicher, G.; Sirringhaus, H. Charge transport in high-mobility conjugated polymers and molecular semiconductors. *Nat. Mater.* **2020**, *19*, 491−502.

(2) Yang, J.; Zhao, Z.; Wang, S.; Guo, Y.; Liu, Y. Insight into High-Performance Conjugated Polymers for Organic Field-Effect Transistors. *Chem* **2018**, *4*, 2748−2785.

(3) Zhang, H.; Liu, K.; Wu, K.-Y.; Chen, Y.-M.; Deng, R.; Li, X.; Jin, H.; Li, S.; Chuang, S. S. C.; Wang, C.-L.; Zhu, Y. Hydrogen-Bonding-Mediated Solid-State Self-Assembled Isoepindolidiones (isoEpi) Crystal for Organic Field-Effect Transistor. *J. Phys. Chem. C* **2018**, *122*, 5888−5895.

(4) Du, T.; Liu, Y.; Wang, C.; Deng, Y.; Geng, Y. n-Type Conjugated Polymers Based on an Indandione-Terminated Quinoidal Building Block. *Macromolecules* **2022**, *55*, 5975−5984.

(5) Nikolka, M.; Nasrallah, I.; Rose, B.; Ravva, M. K.; Broch, K.; Sadhanala, A.; Harkin, D.; Charmet, J.; Hurhangee, M.; Brown, A.; Illig, S.; Too, P.; Jongman, J.; McCulloch, I.; Bredas, J. L.; Sirringhaus, H. High operational and environmental stability of high-mobility

conjugated polymer field-effect transistors through the use of molecular additives. *Nat. Mater.* **2017**, *16*, 356−362.
(6) Lei, T.; Cao, Y.; Fan, Y.; Liu, C. J.; Yuan, S. C.; Pei, J. High-performance air-stable organic field-effect transistors: isoindigo-based conjugated polymers. *J. Am. Chem. Soc.* **2011**, *133*, 6099−6101.
(7) Feng, S.; Li, M.; Tang, N.; Wang, X.; Huang, H.; Ran, G.; Liu, Y.; Xie, Z.; Zhang, W.; Bo, Z. Regulating the Packing of Non-Fullerene Acceptors via Multiple Noncovalent Interactions for Enhancing the Performance of Organic Solar Cells. *ACS Appl. Mater. Interfaces* **2020**, *12*, 4638−4648.
(8) Fan, B.; Zhang, K.; Jiang, X. F.; Ying, L.; Huang, F.; Cao, Y. High-Performance Nonfullerene Polymer Solar Cells based on Imide-Functionalized Wide-Bandgap Polymers. *Adv. Mater.* **2017**, *29*, No. e1606369.
(9) Zhang, C.; Xu, C.; Chen, C.; Cheng, J.; Zhang, H.; Ni, F.; Wang, X.; Zou, G.; Qiu, L. Optically Programmable Circularly Polarized Photodetector. *ACS Nano* **2022**, *16*, 12452−12461.
(10) Wang, C.; Dong, H.; Hu, W.; Liu, Y.; Zhu, D. Semiconducting π-conjugated systems in field-effect transistors: a material odyssey of organic electronics. *Chem. Rev.* **2012**, *112*, 2208−2267.
(11) Roche, G. H.; Tsai, Y.-T.; Clevers, S.; Thuau, D.; Castet, F.; Geerts, Y. H.; Moreau, J. J. E.; Wantz, G.; Dautel, O. J. The role of H-bonds in the solid state organization of [1]benzothieno[3,2-b][1]benzothiophene (BTBT) structures: bis(hydroxy-hexyl)-BTBT, as a functional derivative offering efficient air stable organic field effect transistors (OFETs). *J. Mater. Chem. C* **2016**, *4*, 6742−6749.
(12) Mula, S.; Han, T.; Heiser, T.; Leveque, P.; Leclerc, N.; Srivastava, A. P.; Ruiz-Carretero, A.; Ulrich, G. Hydrogen Bonding as a Supramolecular Tool for Robust OFET Devices. *Chem. - Eur. J.* **2019**, *25*, 8304−8312.
(13) Liu, Y.; Zhang, Z.; Feng, S.; Li, M.; Wu, L.; Hou, R.; Xu, X.; Chen, X.; Bo, Z. Exploiting Noncovalently Conformational Locking as a Design Strategy for High Performance Fused-Ring Electron Acceptor Used in Polymer Solar Cells. *J. Am. Chem. Soc.* **2017**, *139*, 3356−3359.
(14) Zhang, Q.; Huang, J.; Wang, K.; Huang, W. Recent Structural Engineering of Polymer Semiconductors Incorporating Hydrogen Bonds. *Adv. Mater.* **2022**, *34*, No. e2110639.
(15) Ziffer, M. E.; Jo, S. B.; Liu, Y.; Zhong, H.; Mohammed, J. C.; Harrison, J. S.; Jen, A. K. Y.; Ginger, D. S. Tuning H- and J-Aggregate Behavior in π-Conjugated Polymers via Noncovalent Interactions. *J. Phys. Chem. C* **2018**, *122*, 18860−18869.
(16) Zhu, C.; Kalin, A. J.; Fang, L. Covalent and Noncovalent Approaches to Rigid Coplanar π-Conjugated Molecules and Macromolecules. *Acc. Chem. Res.* **2019**, *52*, 1089−1100.
(17) Oh, J. Y.; Rondeau-Gagne, S.; Chiu, Y. C.; Chortos, A.; Lissel, F.; Wang, G. N.; Schroeder, B. C.; Kurosawa, T.; Lopez, J.; Katsumata, T.; Xu, J.; Zhu, C.; Gu, X.; Bae, W. G.; Kim, Y.; Jin, L.; Chung, J. W.; Tok, J. B.; Bao, Z. Intrinsically stretchable and healable semiconducting polymer for organic transistors. *Nature* **2016**, *539*, 411−415.
(18) Yang, K.; He, T.; Chen, X.; Cheng, S. Z. D.; Zhu, Y. Patternable Conjugated Polymers with Latent Hydrogen-Bonding on the Main Chain. *Macromolecules* **2014**, *47*, 8479−8486.
(19) Ruiz-Carretero, A.; Ávila Rovelo, N. R.; Militzer, S.; Mésini, P. J. Hydrogen-bonded diketopyrrolopyrrole derivatives for energy-related applications. *J. Mater. Chem. A* **2019**, *7*, 23451−23475.
(20) Huang, H.; Yang, L.; Facchetti, A.; Marks, T. J. Organic and Polymeric Semiconductors Enhanced by Noncovalent Conformational Locks. *Chem. Rev.* **2017**, *117*, 10291−10318.
(21) Zheng, Y.; Ashizawa, M.; Zhang, S.; Kang, J.; Nikzad, S.; Yu, Z.; Ochiai, Y.; Wu, H.-C.; Tran, H.; Mun, J.; Zheng, Y.-Q.; Tok, J. B. H.; Gu, X.; Bao, Z. Tuning the Mechanical Properties of a Polymer Semiconductor by Modulating Hydrogen Bonding Interactions. *Chem. Mater.* **2020**, *32*, 5700−5714.
(22) Yao, J.; Yu, C.; Liu, Z.; Luo, H.; Yang, Y.; Zhang, G.; Zhang, D. Significant Improvement of Semiconducting Performance of the Diketopyrrolopyrrole-Quaterthiophene Conjugated Polymer through Side-Chain Engineering via Hydrogen-Bonding. *J. Am. Chem. Soc.* **2016**, *138*, 173−185.
(23) Ocheje, M. U.; Selivanova, M.; Zhang, S.; Van Nguyen, T. H.; Charron, B. P.; Chuang, C.-H.; Cheng, Y.-H.; Billet, B.; Noori, S.; Chiu, Y.-C.; Gu, X.; Rondeau-Gagné, S. Influence of amide-containing side chains on the mechanical properties of diketopyrrolopyrrole-based polymers. *Polym. Chem.* **2018**, *9*, 5531−5542.
(24) Ocheje, M. U.; Charron, B. P.; Cheng, Y.-H.; Chuang, C.-H.; Soldera, A.; Chiu, Y.-C.; Rondeau-Gagné, S. Amide-Containing Alkyl Chains in Conjugated Polymers: Effect on Self-Assembly and Electronic Properties. *Macromolecules* **2018**, *51*, 1336−1344.
(25) Lee, M. Y.; Dharmapurikar, S.; Lee, S. J.; Cho, Y.; Yang, C.; Oh, J. H. Regular H-Bonding-Containing Polymers with Stretchability up to 100% External Strain for Self-Healable Plastic Transistors. *Chem. Mater.* **2020**, *32*, 1914−1924.
(26) Galuska, L. A.; Ocheje, M. U.; Ahmad, Z. C.; Rondeau-Gagné, S.; Gu, X. Elucidating the Role of Hydrogen Bonds for Improved Mechanical Properties in a High-Performance Semiconducting Polymer. *Chem. Mater.* **2022**, *34*, 2259−2267.
(27) Charron, B. P.; Ocheje, M. U.; Selivanova, M.; Hendsbee, A. D.; Li, Y.; Rondeau-Gagné, S. Electronic properties of isoindigo-based conjugated polymers bearing urea-containing and linear alkyl side chains. *J. Mater. Chem. C* **2018**, *6*, 12070−12078.
(28) Gasperini, A.; Wang, G.-J. N.; Molina-Lopez, F.; Wu, H.-C.; Lopez, J.; Xu, J.; Luo, S.; Zhou, D.; Xue, G.; Tok, J. B. H.; Bao, Z. Characterization of Hydrogen Bonding Formation and Breaking in Semiconducting Polymers under Mechanical Strain. *Macromolecules* **2019**, *52*, 2476−2486.
(29) Huang, J.; Pan, Y.; Chen, Z.; Zhang, W.; Yu, G. Ethanediylidenebis(isoquinolinedione): A Six-Membered-Ring Diimide Building Block for Ambipolar Semiconducting Polymers. *Macromolecules* **2019**, *52*, 8238−8247.
(30) Huang, J.; Yu, G. Structural Engineering in Polymer Semiconductors with Aromatic N-Heterocycles. *Chem. Mater.* **2021**, *33*, 1513−1539.
(31) Fei, Z.; Han, Y.; Martin, J.; Scholes, F. H.; Al-Hashimi, M.; AlQaradawi, S. Y.; Stingelin, N.; Anthopoulos, T. D.; Heeney, M. Conjugated Copolymers of Vinylene Flanked Naphthalene Diimide. *Macromolecules* **2016**, *49*, 6384−6393.
(32) Lei, T.; Xia, X.; Wang, J. Y.; Liu, C. J.; Pei, J. "Conformation locked" strong electron-deficient poly(p-phenylene vinylene) derivatives for ambient-stable n-type field-effect transistors: synthesis, properties, and effects of fluorine substitution position. *J. Am. Chem. Soc.* **2014**, *136*, 2135−2141.
(33) Liu, B.; Li, J.; Zeng, W.; Yang, W.; Yan, H.; Li, D.-c.; Zhou, Y.; Gao, X.; Zhang, Q. High-Performance Organic Semiconducting Polymers by a Resonance-Assisted Hydrogen Bonding Approach. *Chem. Mater.* **2021**, *33*, 580−588.
(34) Bronstein, H.; Frost, J. M.; Hadipour, A.; Kim, Y.; Nielsen, C. B.; Ashraf, R. S.; Rand, B. P.; Watkins, S.; McCulloch, I. Effect of Fluorination on the Properties of a Donor−Acceptor Copolymer for Use in Photovoltaic Cells and Transistors. *Chem. Mater.* **2013**, *25*, 277−285.
(35) Kim, H. S.; Huseynova, G.; Noh, Y.-Y.; Hwang, D.-H. Modulation of Majority Charge Carrier from Hole to Electron by Incorporation of Cyano Groups in Diketopyrrolopyrrole-Based Polymers. *Macromolecules* **2017**, *50*, 7550−7558.
(36) Wei, C.; Zhang, W.; Huang, J.; Li, H.; Zhou, Y.; Yu, G. Realizing n-Type Field-Effect Performance via Introducing Trifluoromethyl Groups into the Donor−Acceptor Copolymer Backbone. *Macromolecules* **2019**, *52*, 2911−2921.
(37) Ocheje, M. U.; Goodman, R. B.; Lu, K.-T.; Wang, Y.; Galuska, L. A.; Soullard, L.; Cao, Z.; Zhang, S.; Yadiki, M.; Gu, X.; Chiu, Y.-C.; Rondeau-Gagné, S. Precise Control of Noncovalent Interactions in Semiconducting Polymers for High-Performance Organic Field-Effect Transistors. *Chem. Mater.* **2021**, *33*, 8267−8277.
(38) Chen, Z.; Zhang, W.; Huang, J.; Gao, D.; Wei, C.; Lin, Z.; Wang, L.; Yu, G. Fluorinated Dithienylethene−Naphthalenediimide

Copolymers for High-Mobility n-Channel Field-Effect Transistors. *Macromolecules* **2017**, *50*, 6098−6107.
(39) Faghihnejad, A.; Feldman, K. E.; Yu, J.; Tirrell, M. V.; Israelachvili, J. N.; Hawker, C. J.; Kramer, E. J.; Zeng, H. Adhesion and Surface Interactions of a Self-Healing Polymer with Multiple Hydrogen-Bonding Groups. *Adv. Funct. Mater.* **2014**, *24*, 2322−2333.
(40) Gao, W.; Tang, R.; Bai, M.; Yu, H.; Ruan, Y.; Zheng, J.; Chen, Y.; Weng, W. Dynamic covalent polymer networks with mechanical and mechanoresponsive properties reinforced by strong hydrogen bonding. *Polym. Chem.* **2022**, *13*, 2173−2177.
(41) Zhang, G.; Yang, Y.; Chen, Y.; Huang, J.; Zhang, T.; Zeng, H.; Wang, C.; Liu, G.; Deng, Y. A Quadruple-Hydrogen-Bonded Supramolecular Binder for High-Performance Silicon Anodes in Lithium-Ion Batteries. *Small* **2018**, *14*, No. e1801189.
(42) Verjans, J.; André, A.; Van Ruymbeke, E.; Hoogenboom, R. Physically Cross-Linked Polybutadiene by Quadruple Hydrogen Bonding through Side-Chain Incorporation of Ureidopyrimidinone with Branched Alkyl Side Chains. *Macromolecules* **2022**, *55*, 928−941.
(43) Song, P.; Wang, H. High-Performance Polymeric Materials through Hydrogen-Bond Cross-Linking. *Adv. Mater.* **2020**, *32*, No. e1901244.
(44) Chen, X.; Zawaski, C. E.; Spiering, G. A.; Liu, B.; Orsino, C. M.; Moore, R. B.; Williams, C. B.; Long, T. E. Quadruple Hydrogen Bonding Supramolecular Elastomers for Melt Extrusion Additive Manufacturing. *ACS Appl. Mater. Interfaces* **2020**, *12*, 32006−32016.
(45) Pan, Y.; Hu, J.; Yang, Z.; Tan, L. From Fragile Plastic to Room-Temperature Self-Healing Elastomer: Tuning Quadruple Hydrogen Bonding Interaction through One-Pot Synthesis. *ACS Appl. Polym. Mater.* **2019**, *1*, 425−436.
(46) Song, Y.; Liu, Y.; Qi, T.; Li, G. L. Towards Dynamic but Supertough Healable Polymers through Biomimetic Hierarchical Hydrogen-Bonding Interactions. *Angew. Chem., Int. Ed.* **2018**, *57*, 13838−13842.
(47) Yan, X.; Liu, Z.; Zhang, Q.; Lopez, J.; Wang, H.; Wu, H. C.; Niu, S.; Yan, H.; Wang, S.; Lei, T.; Li, J.; Qi, D.; Huang, P.; Huang, J.; Zhang, Y.; Wang, Y.; Li, G.; Tok, J. B.; Chen, X.; Bao, Z. Quadruple H-Bonding Cross-Linked Supramolecular Polymeric Materials as Substrates for Stretchable, Antitearing, and Self-Healable Thin Film Electrodes. *J. Am. Chem. Soc.* **2018**, *140*, 5280−5289.
(48) Yen, H.-C.; Lin, Y.-C.; Chen, W.-C. Modulation of the Hydrophilicity on Asymmetric Side Chains of Isoindigo-Based Polymers for Improving Carrier Mobility−Stretchability Properties. *Macromolecules* **2021**, *54*, 1665−1676.
(49) Lin, Y. C.; Huang, Y. W.; Hung, C. C.; Chiang, Y. C.; Chen, C. K.; Hsu, L. C.; Chueh, C. C.; Chen, W. C. Backbone Engineering of Diketopyrrolopyrrole-Based Conjugated Polymers through Random Terpolymerization for Improved Mobility-Stretchability Property. *ACS Appl. Mater. Interfaces* **2020**, *12*, 50648−50659.
(50) Chen, J.; Li, F.; Luo, Y.; Shi, Y.; Ma, X.; Zhang, M.; Boukhvalov, D. W.; Luo, Z. A self-healing elastomer based on an intrinsic non-covalent cross-linking mechanism. *J. Mater. Chem. A* **2019**, *7*, 15207−15214.
(51) Savagatrup, S.; Makaram, A. S.; Burke, D. J.; Lipomi, D. J. Mechanical Properties of Conjugated Polymers and Polymer-Fullerene Composites as a Function of Molecular Structure. *Adv. Funct. Mater.* **2014**, *24*, 1169−1181.
(52) Filiatrault, H. L.; Porteous, G. C.; Carmichael, R. S.; Davidson, G. J.; Carmichael, T. B. Stretchable light-emitting electrochemical cells using an elastomeric emissive material. *Adv. Mater.* **2012**, *24*, 2673−2678.
(53) Zhang, Z.; Cheng, L.; Zhao, J.; Zhang, H.; Zhao, X.; Liu, Y.; Bai, R.; Pan, H.; Yu, W.; Yan, X. Muscle-Mimetic Synergistic Covalent and Supramolecular Polymers: Phototriggered Formation Leads to Mechanical Performance Boost. *J. Am. Chem. Soc.* **2021**, *143*, 902−911.

https://doi.org/10.1021/acs.macromol.3c00443
Macromolecules 2023, 56, 5369−5380